UCSF
UC San Francisco Previously Published Works

Title

Directed Evolution of Brain-Derived Neurotrophic Factor for Improved Folding and Expression in Saccharomyces cerevisiae

Permalink

https://escholarship.org/uc/item/7d30370c

Journal

Applied and Environmental Microbiology, 80(18)

ISSN

0099-2240

Authors

Burns, Michael L
Malott, Thomas M
Metcalf, Kevin J
et al.

Publication Date

2014-09-15

DOI

10.1128/aem.01466-14

Peer reviewed

eScholarship.org Powered by the California Digital Library
University of California

AEM
Journals.ASM.org

Directed Evolution of Brain-Derived Neurotrophic Factor for Improved Folding and Expression in *Saccharomyces cerevisiae*

Michael L. Burns,[a] Thomas M. Malott,[a] Kevin J. Metcalf,[a] Benjamin J. Hackel,[b] Jonah R. Chan,[c] Eric V. Shusta[a]

Department of Chemical and Biological Engineering, University of Wisconsin—Madison, Madison, Wisconsin, USA[a]; Department of Chemical Engineering and Materials Science, University of Minnesota, Minneapolis, Minnesota, USA[b]; Department of Neurology, Program in Neuroscience, University of California, San Francisco, San Francisco, California, USA[c]

Brain-derived neurotrophic factor (BDNF) plays an important role in nervous system function and has therapeutic potential. Microbial production of BDNF has resulted in a low-fidelity protein product, often in the form of large, insoluble aggregates incapable of binding to cognate TrkB or p75 receptors. In this study, employing *Saccharomyces cerevisiae* display and secretion systems, it was found that BDNF was poorly expressed and partially inactive on the yeast surface and that BDNF was secreted at low levels in the form of disulfide-bonded aggregates. Thus, for the purpose of increasing the compatibility of yeast as an expression host for BDNF, directed-evolution approaches were employed to improve BDNF folding and expression levels. Yeast surface display was combined with two rounds of directed evolution employing random mutagenesis and shuffling to identify BDNF mutants that had 5-fold improvements in expression, 4-fold increases in specific TrkB binding activity, and restored p75 binding activity, both as displayed proteins and as secreted proteins. Secreted BDNF mutants were found largely in the form of soluble homodimers that could stimulate TrkB phosphorylation in transfected PC12 cells. Site-directed mutagenesis studies indicated that a particularly important mutational class involved the introduction of cysteines proximal to the native cysteines that participate in the BDNF cysteine knot architecture. Taken together, these findings show that yeast is now a viable alternative for both the production and the engineering of BDNF.

Brain-derived neurotrophic factor (BDNF) is a member of the neurotrophin family that substantially influences mammalian neuronal function from development through adulthood (1). BDNF has also been posited to play a role in brain trauma and several neurodegenerative disorders, including Alzheimer's and Parkinson's diseases (2). As demonstrations of its potential as a therapeutic, BDNF has been shown to be neuroprotective in stroke (3), Alzheimer's disease (4), Parkinson's disease (5), Huntington's disease (6), and peripheral nerve injury (7). BDNF elicits its biological functions through specific interactions with the tropomyosin receptor kinase B (TrkB) and p75 neurotrophin receptors (8, 9), and it is biologically active as a homodimeric protein formed through hydrophobic interactions between the cores of the monomers (10–12). Moreover, each 122-amino-acid monomer of BDNF possesses three intramolecular disulfide bonds in a cysteine knot configuration. These complex folding and assembly requirements governing the production of BDNF and other highly homologous neurotrophin family members, such as nerve growth factor (NGF), have resulted in low heterologous productivity (13), likely as a by-product of the aggregation-prone nature of these proteins (14).

Platforms for neurotrophin production include immortalized mammalian cell lines (13), bacteria (15), insect cell lines (16), and *Saccharomyces cerevisiae* (17). In particular, microbial hosts such as bacteria and yeast have the advantages of facile genetic modification, robust scaling, and comparatively low cost. However, previous attempts to produce BDNF in *Escherichia coli* have yielded mainly insoluble proteins with mismatched disulfide bonds that required isolation and refolding, and even after refolding, the biological activity was attenuated (15, 18). As a partial resolution, bacterial host engineering in the form of co-overexpression of Dsb disulfide-bonding machinery in bacteria could raise the level of soluble BDNF production to 35% (15). Similarly, despite the eukaryotic protein-folding and -processing machinery of yeast, NGF production in yeast yielded a low-fidelity product (17). Here we report that yeast also produces BDNF primarily in an inactive and misfolded form. Yeast surface display has been used to identify better-folded and -secreted variants of single-chain T-cell receptors (19), antibody Fc regions (20), and epidermal growth factor receptor (21), among others (22). Thus, yeast surface display approaches were employed to improve the protein-folding and -processing properties of BDNF. Two rounds of directed evolution (DE) were used to identify mutations that resulted in better specific binding activity of BDNF toward both TrkB and p75, along with higher expression levels on the yeast surface. Subsequently, the mutants led to substantially improved secretion titers and specific receptor binding activity compared to wild-type BDNF, and the top-performing BDNF mutants were demonstrated to be capable of triggering TrkB receptor phosphorylation.

MATERIALS AND METHODS

Strains, plasmids, materials, and media. An open reading frame encoding residues 1 to 119 of mature human BDNF was subcloned into the pCT-ESO yeast display vector (23) to drive yeast display of BDNF as a fusion to the yeast mating protein agglutinin, Aga2p. The resultant pCT-

Received 6 May 2014 Accepted 7 July 2014
Published ahead of print 11 July 2014
Editor: A. A. Brakhage
Address correspondence to Eric V. Shusta, shusta@engr.wisc.edu.
Supplemental material for this article may be found at http://dx.doi.org/10.1128/AEM.01466-14.
Copyright © 2014, American Society for Microbiology. All Rights Reserved.
doi:10.1128/AEM.01466-14

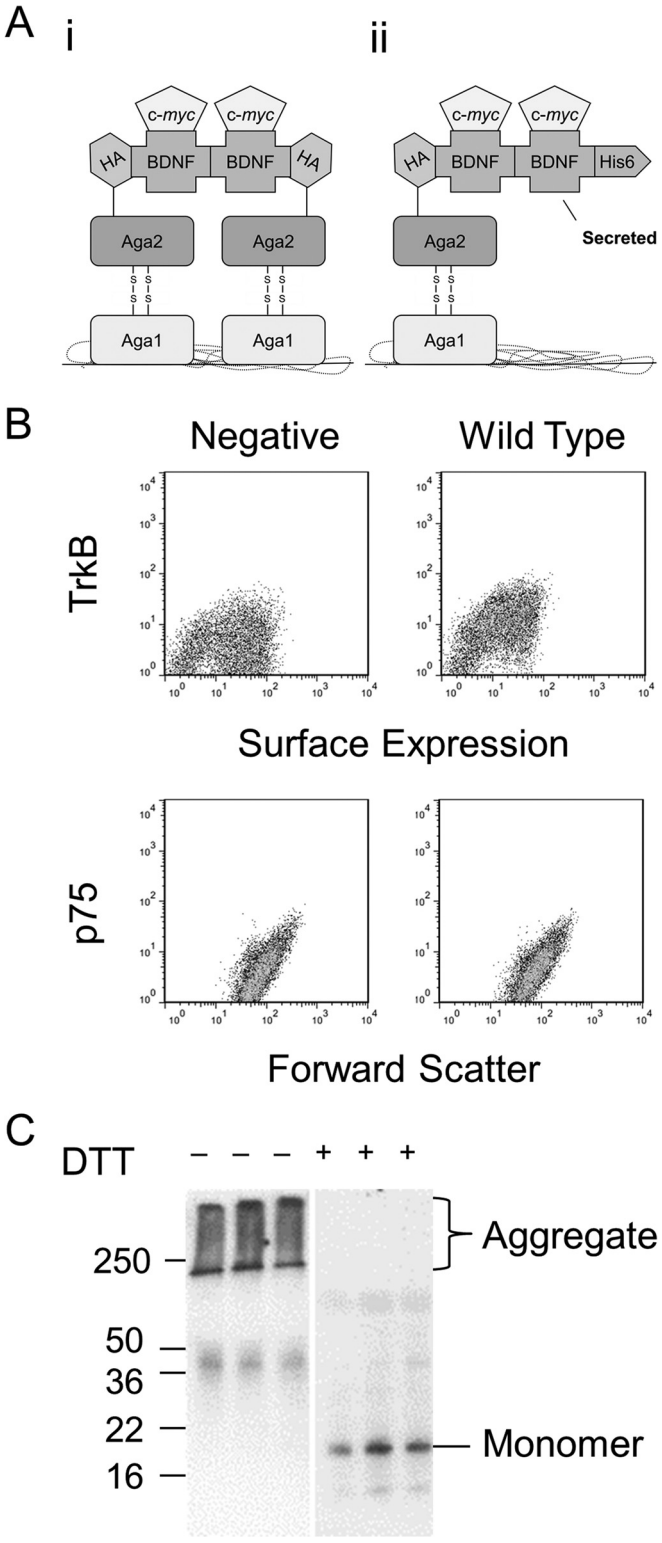

FIG 1 Production of BDNF using yeast. (A) Schematics of BDNF constructs displayed on the yeast surface as a dimer of two surface display proteins (i) and as a dimer of one surface display protein and one secreted and captured protein (ii). (B) Expression and receptor-binding properties of wild-type BDNF displayed on the yeast surface using scheme i. Shown are sample flow cytometric dot plots of surface-displayed wild-type BDNF either colabeled with its natural receptor TrkB and an anti-c-*myc* antibody to monitor full-length expression or labeled with p75 alone. The negative sample is yeast displaying an irrelevant single-chain antibody labeled in the exact same manner as the BDNF sample. Note the presence of a full-length single-chain antibody on the yeast surface but the absence of TrkB and p75 labeling. Quantified data are reported in Table 2. (C) Western blots of secreted wild-type BDNF with (+) or without (−) reduction by DTT. Supernatants from triplicate independent transformants were analyzed. Molecular sizes (in kDa) are indicated on the left.

ESO-BDNF construct encoded Aga2p-HA-BDNF-c-*myc* (Fig. 1A). Similarly, the mature human BDNF open reading frame was subcloned into pRS316-GFP (24) for yeast secretion, yielding pRS316-BDNF, encoding BDNF-c-*myc*-His_6. The anti-fluorescein single-chain antibody 4-4-20 was used as a control for some experiments (25). Control strains were created using empty plasmids containing nutritional markers alone (pRS-314, pRS-316). Vectors were transformed into the yeast secretion strain BJ5464 (Yeast Genetic Stock Center, Berkeley, CA, USA), the yeast display strain EBY100 (26), and the yeast display strain AWY100 (25), as appropriate. All transformations were performed using the lithium acetate method (27) and yeast grown in minimal medium (2% dextrose, 0.67% yeast nitrogen base) buffered at pH 6.0 with 50 mM sodium phosphate and containing either 1% Casamino Acids (CAA [Becton Dickinson, Franklin Lakes, NJ, USA]; lacking tryptophan and uracil) to yield SD-CAA or 2× synthetic amino acid supplement (SCAA; containing 190 mg/liter Arg, 108 mg/liter Met, 52 mg/liter Tyr, 290 mg/liter Ile, 440 mg/liter Lys, 200 mg/liter Phe, 1,260 mg/liter Glu, 400 mg/liter Asp, 480 mg/liter Val, 220 mg/liter Thr, and 130 mg/liter Gly and lacking leucine, tryptophan, and uracil) to yield SD-SCAA. Leucine (200 mg/liter), tryptophan (20 mg/liter), and uracil (20 mg/liter) were added when necessary for proper auxotrophic selection. Protein display and secretion were induced in the same media, with the dextrose replaced by 2% galactose (yielding SG-CAA or SG-SCAA). Fresh transformants were used in all experiments.

Surface display binding and affinity measurements. For surface display, yeast clones were first grown in SD-CAA at 30°C to an optical density at 600 nm (OD_{600}) of 1.0 and then induced for display in an equal volume of SG-CAA for 18 h at 20°C. Ice cold phosphate-buffered saline (PBS) with 1 mg/ml bovine serum albumin (BSA) at pH 7.4 (PBS-BSA) was used in all washes and was included in primary and secondary antibody labeling solutions. Yeast cells (2×10^6) were collected, washed in PBS-BSA, and immunolabeled for flow cytometric analysis. Immunolabeling was conducted for 30 min at 4°C using the following primary labels: anti-c-*myc* epitope antibody 9e10 (30 to 50 μg/ml; Covance, CA, USA), anti-hemagglutinin (anti-HA) epitope antibody 12Ca5 (25 μg/ml; Roche, IN, USA), an anti-His_4 antibody (2 μg/ml; Qiagen, CA, USA), a recombinant human TrkB–Fc chimera (TrkB) (5 μg/ml; R&D Systems, MN, USA), and a recombinant human NGF receptor–tumor necrosis factor receptor superfamily 16 (TNFRSF16)–Fc chimera (p75) (5 μg/ml; R&D Systems). After three washes with PBS-BSA, the following secondary labels were applied for 30 min at 4°C: anti-human immunoglobulin G (IgG) conjugated to phycoerythrin (PE) (1:45; Sigma, St. Louis, MO, USA) for TrkB and p75 detection and anti-mouse IgG conjugated to Alexa Fluor 488 (1:500; Invitrogen, CA, USA) for c-*myc*, HA, and His_6 detection. Following three washes with PBS-BSA, cells were analyzed on a Becton Dickinson FACSCalibur benchtop flow cytometer. Geometric means for the positive populations were corrected by subtracting the geometric means for the nondisplaying yeast population. When there was peak overlap between the displaying and nondisplaying populations, peak deconvolution methods were employed as described previously (28). In many cases, the TrkB and p75 binding signals were subsequently divided by the anti-c-*myc* signal to represent the data as the level of binding per molecule.

Dimer determination using flow cytometry was performed using cotransformation of selected plasmids pRS316-BDNF (secreted BDNF with a His_6 tag) and pCT-ESO-BDNF (display without a His_6 tag) into the AWY100 yeast surface display strain. His_6 labeling, and hence surface capture by dimerization, was determined using the anti-His_4 antibody (2 μg/ml; Qiagen).

Apparent affinity measurements were determined in surface display

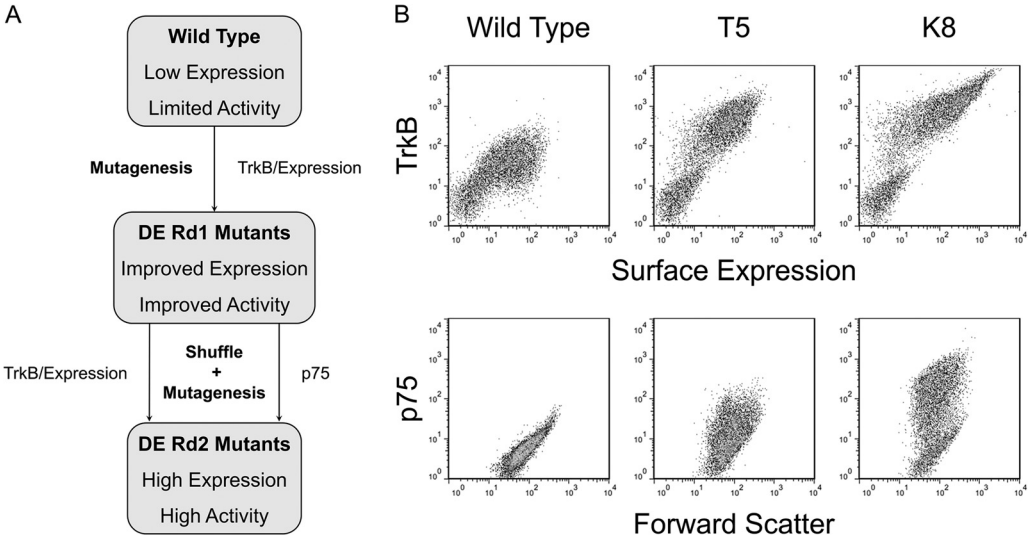

FIG 2 Directed evolution of BDNF. (A) Flow chart of the directed-evolution process showing outcomes and screening criteria. (B) Flow cytometric data illustrating the directed-evolution improvement in BDNF activity (TrkB and p75) and full-length expression (anti-c-*myc* antibody) as a surface-displayed protein. Mutant T5 is shown as an example of DE Rd1 mutants and mutant K8 as an example of DE Rd2 mutants. Quantified data for all DE Rd1 and Rd2 mutants assessed are displayed in Table 2.

format using the serially diluted TrkB receptor diluted in PBS-BSA. Flow cytometric geometric mean fluorescent signals were adjusted for background fluorescence. Apparent binding affinity (K_D) calculations were then made using a nonlinear least-squares estimation for single-receptor–single-ligand binding using Athena Visual as described previously (29). All statistical comparisons throughout this study were performed using an unpaired, two-tailed Student *t* test.

BDNF library construction and screening. Mutagenic libraries were constructed as described previously (21, 30, 31). Briefly, in both directed evolution (DE) round 1 (Rd1) and Rd2, a BDNF mutant library was generated by error-prone PCR using the triphosphate derivatives of nucleotide analogs 2′-deoxy-*p*-nucleoside-5′-triphosphate and 8-oxo-2′-deoxyguanosine-5′-triphosphate (TriLink BioTechnologies, San Diego, CA, USA) (32). Mutated BDNF open reading frames derived from several error-prone PCRs with varying analog concentrations and PCR cycles were combined and were introduced into a digested pCT-ESO acceptor vector by homologous recombination. A library of 4×10^6 transformants resulted for DE Rd1. Sequencing of 20 randomly selected clones prior to sorting indicated a total mutation rate of approximately 0.2 to 3.8%, or between 1 and 14 base pair changes per BDNF mutant. For DE Rd2, a 1:1 mixture of individual clones isolated from DE Rd1 and wild-type BDNF was digested with DNase I to yield fragments of 10 to 100 bp, which were shuffled as described previously (33) and were simultaneously subjected to a low rate of additional mutagenesis using nucleotide analogs. This second-round library comprised 1.1×10^7 transformants.

Libraries were grown in selective media at 30°C to an OD_{600} of 1.0 and were induced for 18 h at 20°C. Surface display labeling was conducted as described above using a number of induced cells that was 10 times the library size. The overall directed-evolution screening strategy is depicted in Fig. 2A. For DE Rd1, the library was screened using both folding/activity (with the TrkB receptor) and expression (sorting rounds 1 and 3 used an anti-c-*myc* antibody, and sorting round 2 used an anti-HA antibody). Saturating concentrations of the TrkB receptor were employed to bias the screen toward folding fidelity rather than affinity improvements. TrkB concentrations of 5 μg/ml (35 nM) were validated as saturating by using wild-type BDNF-displaying yeast. Cells were sorted using a Becton Dickinson FACSVantage SE flow cytometric sorter at the University of Wisconsin Comprehensive Cancer Center. Sort gates were set to collect dual-positive high-fluorescence events, and stringency was increased between sorting rounds (from 2.0 to 0.5% of the total population). Sorted yeast cells were maintained for 1 passage in SD-CAA medium with 50 mM citrate replacing phosphate and with 25 mg/liter kanamycin (Sigma). The recovered pools were subsequently passaged into standard SD-CAA medium and were induced for the next round of sorting as described above for the initial library. Individual clones were isolated from a population and analyzed by plating on nutritionally selective plates; they were designated "T" or "B" simply because they came from different stringency sort gates in the final round of sorting. Plasmid DNA was recovered from yeast colonies using the Zymoprep II yeast plasmid miniprep kit (Zymo Research, CA, USA), amplified in DH5α cells (Invitrogen), and sequenced at the University of Wisconsin Biotechnology Center in order to determine mutagenic alterations. Retransformation into the parental display strain EBY100 confirmed that the improvements in folding, activity, and expression were due to the mutated BDNF genes harbored.

DE Rd2 consisted of four sorting rounds, again using increasing stringency (2.0 to 0.5%). In the first sort of DE Rd2, the library was labeled with TrkB in combination with an anti-c-*myc* antibody. After this sort, the pool was further sorted along parallel paths, either continuing with TrkB plus the anti-c-*myc* antibody or employing p75 labeling alone, for three additional rounds. The individual clones isolated from sorting for all four rounds using TrkB and anti-c-*myc* were designated "K" mutants, while those recovered from sorting in the last three rounds using p75 were designated "P" mutants.

Protein secretion and purification. Yeast cultures harboring the pRS-316-BDNF plasmids were grown 1 to 2 days in minimal medium at 30°C, diluted to a uniform OD_{600} of 0.1, and grown for 2 additional days at 30°C. Protein expression was induced by switching to SG-CAA (with 1 mg/ml BSA as a nonspecific carrier) at 20°C for 3 days. Cell-free supernatants were then collected for Western blot analysis, ELISA analysis, or purification.

For protein purification, 50-ml yeast cultures were grown and induced for protein secretion. The K8, P10, or pRS-316 mock-transfected supernatants were dialyzed twice overnight at 4°C against 2 liters PBS, pH 8.0. The dialyzed His_6-tagged protein material was then batch purified using 250 μl Superflow Ni-nitrilotriacetic acid (NTA) beads (Qiagen). The BDNF-loaded beads were washed three times in 750 μl of a wash buffer containing 20 mM imidazole (6.9 g/liter NaH_2PO_4-H_2O, 17.5 g/liter NaCl, 1.36 g/liter imidazole [pH 8.0]), and BDNF was recovered using an

elution buffer containing 250 mM imidazole (6.9 g/liter NaH_2PO_4-H_2O, 17.5 g/liter NaCl, 17 g/liter imidazole [pH 8.0]). The purified material was stored for as long as 2 weeks at 4°C prior to use in activity experiments with no noticeable loss of activity in a TrkB binding ELISA.

Western blotting. Western blotting was performed as described previously (24). Briefly, secreted BDNF in the form of supernatants and purified proteins was resolved by reducing SDS-polyacrylamide gel electrophoresis (PAGE) using either 12.5% or 10-to-20% Tris-glycine minigradient gels (Invitrogen). Nonreducing Western blotting was performed as described above, but in the absence of dithiothreitol (DTT). Resolved proteins were transferred to nitrocellulose membranes, which were probed with primary antibody 9e10 (dilution, 1:3,000; Covance) and a horseradish peroxidase (HRP)-conjugated anti-mouse secondary antibody (1:2,000; Sigma), followed by enhanced chemiluminescence detection with the Amersham ECL system and exposure to Amersham Hyperfilm ECL. Films at various exposure times were analyzed with ImageJ software to determine band intensities, and the slope of the intensity-versus-exposure time curve in the unsaturated, linear region was then utilized to determine relative protein concentrations in the supernatants. The values were then normalized to the culture density (OD_{600}) and hence represent relative per-cell secretion levels.

Absolute protein concentrations for secreted BDNF mutants K8 and P10 were determined to be 1 mg/liter as measured by Western blotting with an anti-BDNF primary antibody (1:750; Promega) and an HRP-conjugated anti-chicken secondary antibody (1:4,000; Promega) with comparison to the BDNF standard (50 ng/ml; PeproTech).

TrkB and p75 ELISA. Enzyme-linked immunosorbent assays (ELISA) were used to determine the binding activity of the secreted BDNF protein. Nunc-Immuno 96-well MaxiSorp plates (Nunc, NY, USA) were coated with the TrkB-Fc or p75-Fc receptor (10 μg/ml; R&D Systems) overnight at 4°C and were blocked for 2 h with 250 μl PBS-BT (PBS at pH 7.4 with 1 mg/ml BSA and 0.1% Tween 20). One hundred microliters of the BDNF supernatant dilution series was added at 4°C for 1 h. The BDNF protein standard (PeproTech, NJ, USA) was used as a positive control. Wells were washed four times with 250 μl PBS-BT between all labeling steps. Captured BDNF was detected by labeling with the primary anti-c-*myc* antibody 9e10 (10 μg/ml; Covance) for 30 min at 4°C and subsequent labeling with the HRP-conjugated secondary anti-mouse antibody (1:2,000; Sigma) for 30 min at 4°C. Samples were incubated with 100 μl of the tetramethylbenzidine two-component microwell peroxidase substrate kit (Kirkegaard & Perry Laboratories, MD, USA). The reaction was stopped with 100 μl of 2 M H_3PO_4, and absorbance at 450 nm was measured. Data in the linear range of supernatant dilution were used to determine the slope of the absorbance-versus-concentration curve. The slope was then normalized by the amount of total BDNF protein in the ELISA sample as determined by quantitative Western blotting with the c-*myc* epitope to yield the specific activity to the TrkB or p75 receptor (i.e., TrkB ELISA activity/c-*myc* Western blot signal or p75 ELISA activity/c-*myc* Western blot signal).

SEC. A Superdex 75 10/300 GL (GE Healthcare, Sweden) size exclusion column and a BioCAD 700E chromatography workstation (PerSeptive Biosystems, MN, USA) were used for size exclusion chromatography (SEC). Samples were run at 0.5 ml/min using either 250 μl gel filtration standard (Bio-Rad, CA, USA) or 300 μl purified K8. Samples were collected from the column at 1-min intervals, and eluates were subjected to chemical cross-linking by the addition of 0.1% glutaraldehyde (Fisher Scientific, GA, USA) for 1 h at room temperature. Cross-linking was quenched using a 2 M Tris–0.1 M NaOH solution. Eluates with and without cross-linking were then evaluated by Western blotting under reducing conditions with anti-c-*myc* detection as described above.

PC12 phosphorylation. BDNF-dependent tyrosine phosphorylation of TrkB receptors was performed as described previously (13, 34, 35). Briefly, PC12 cells stably transfected with rat TrkB (36) were grown to confluence in poly-L-lysine (0.1 mg/ml; Sigma)-coated T75 flasks in a culture medium (Dulbecco's modified Eagle medium [DMEM]; Sigma) supplemented with 10% horse serum (Sigma), 5% fetal bovine serum (Sigma), 100 U/ml penicillin, 100 μg/ml streptomycin, 2 mM L-glutamine (Sigma), and 200 μg/ml G418 (Sigma) at 37°C. Two confluent T75 flasks per sample were prepared by starvation in a serum-free medium for 30 min. The BDNF standard (100 ng/ml; PeproTech) or purified K8 or P10 was added at 450 ng/ml. To each T75 flask, 2 ml of BDNF-containing samples was added, and the mixture was incubated for 5 min at 37°C. The flasks were then washed with ice-cold PBS, pH 7.4, and the contents were lysed at 4°C in 1 ml radioimmunoprecipitation buffer (50 mM Tris [pH 7.4], 150 mM NaCl, 1% Triton X-100, 0.5% sodium deoxycholate, 0.1% SDS, 2 mM EDTA, 2.5 mM NaF) containing 1 mM phenylmethylsulfonyl fluoride (PMSF; Roche), 1 mM sodium orthovanadate (Sigma), and complete protease inhibitors (Calbiochem-Novabiochem Corp., CA, USA). The lysates were subsequently immunoprecipitated with 1 μg rabbit anti-pan-Trk IgG (C-14; Santa Cruz Biotechnology, CA, USA) at 4°C for 2 h. To this mixture, 25 μl of cross-linked 6% protein A beaded agarose supplied as a 50% slurry (Pierce, IL, USA) was added, and the mixture was incubated at 4°C for 1 to 2 h. Samples were washed 3 times with 1 ml ice-cold lysis buffer and once with 1 ml ice-cold sterile double-distilled water (ddH_2O). Immunoprecipitated complexes were eluted using 1× Laemmli loading buffer and boiling for 5 min, separated on 8% SDS-PAGE gels (Invitrogen), and transferred to nitrocellulose membranes with overnight blocking in 5% milk. Blots were probed either overnight with anti-phospho-Trk (1:1,000; Cell Signaling Technology, MA, USA) or for 1.5 h with anti-pan-Trk IgG (C-14; Santa Cruz) and an HRP-conjugated anti-rabbit secondary antibody (1:10,000; Sigma). While these experiments were employed to test the abilities of K8 and P10 to drive TrkB phosphorylation, investigation of a single BDNF concentration did not allow a quantitative comparison of specific TrkB phosphorylation activities for K8 and P10.

RESULTS

Creation of a BDNF scaffold capable of binding its natural receptors. BDNF was displayed on the yeast cell surface by standard fusion to the C terminus of the a-agglutinin subunit Aga2p (Fig. 1Ai), and full-length BDNF was detected on the yeast surface via the c-*myc* tag, albeit at relatively low levels (Fig. 1B). The binding of the surface-displayed protein to its natural receptors, TrkB and p75, was assessed as a measure of proper folding and homodimer assembly. While TrkB binding was detected, binding to p75 was not detected (Fig. 1B). Moreover, BDNF secreted into the culture medium was in the form of disulfide-bonded aggregates, as evidenced by its inability to enter a nonreducing SDS-PAGE gel and by its lack of substantial activity in a TrkB ELISA (Fig. 1C). Combined, these data suggested that secreted BDNF, and to some extent displayed BDNF, was produced in a largely inactive, misfolded form that was in some way capable of evading the yeast quality control machinery.

Therefore, to facilitate BDNF folding and processing in yeast, we engineered BDNF through two successive rounds of directed evolution (Fig. 2A). For directed evolution round 1 (DE Rd1), a randomly mutagenized 4×10^6-member BDNF library was screened using the dual criteria of increased TrkB binding activity and increased cell surface expression (Fig. 2A; see Materials and Methods for details). After three rounds of fluorescence-activated cell sorter (FACS)-based sorting, the enriched pools showed substantial improvements in TrkB binding and full-length expression. Individual BDNF mutants were isolated, sequenced (Table 1), and evaluated for their receptor binding and expression properties (Table 2). On average, the DE Rd1 mutants showed a 4-fold increase in TrkB labeling and a 1.6-fold average increase in full-length expression over wild-type BDNF, indicating an average 2.5-fold increase in receptor binding per molecule (Fig. 2B). Since

TABLE 1 Amino acid alterations in BDNF mutants

Amino acid position	Amino acid[a] in:											
	Wild type	DE Rd1				DE Rd2						
		T4	T5	B2	B5	P1	P3	P5	P10	K3	K6	K8
11	Ser	—	—	—	Cys	Cys	Cys	Cys	Cys	Cys	Cys	—
34	Gly	—	Glu	—	—	Glu	Glu	—	—	Glu	—	Glu
40	Glu	—	—	Asp	—	—	—	—	Asp	—	—	Asp
41	Lys	—	—	Glu	—	—	—	Glu	Glu	—	Glu	Glu
48	Gln	—	—	Arg	—	—	—	Arg	Arg	—	Arg	Arg
50	Lys	—	—	—	—	—	—	—	—	Ala	—	—
61	Met	—	—	—	Thr	—	—	—	—	—	—	—
66	Glu	Gly	—	—	—	Gly	—	Gly	Gly	Gly	—	—
67	Gly	—	Cys	—	—	—	—	—	—	—	—	Cys
73	Lys	—	—	Glu	—	—	—	—	—	—	—	—
83	Thr	—	—	—	—	—	—	—	—	Ala	—	—
95	Lys	—	—	Glu	—	—	—	—	—	—	—	—
108	Ser	Ala	—	—	—	Ala	Ala	Ala	Ala	—	Ala	Ala
115	Ile	—	—	—	—	—	—	Ser	Ser	—	—	—

[a] —, same residue as in the wild type.

the screen and clonal evaluation were performed at a saturating TrkB concentration, these binding-per-molecule values represent "specific activity" for surface-displayed BDNF. Interestingly, while p75 binding was not detected for displayed wild-type BDNF, it became evident in many of the mutants in the DE Rd1 enriched pool. Accordingly, individual DE Rd1 mutants exhibited clear binding to p75 (Fig. 2B; Table 2). Given that p75 was not included in the DE round 1 screening process, and since the p75 and Trk receptors have distinct binding epitopes on neurotrophins (10, 37), these results suggest that the improvements in specific activity resulted from a general improvement in the folding fidelity of the BDNF mutants rather than from an isolated improvement in the vicinity of the TrkB binding site.

Since sequencing revealed nonoverlapping mutations in the unique clones derived from DE Rd 1 (Table 1), it was hypothesized that additional improvements could be achieved by combining these alterations through molecular shuffling. Thus, a second round of directed evolution (DE Rd2) was conducted in which the unique clones isolated from DE Rd1 were shuffled and subjected to a low level of additional mutagenesis. Since folding fidelity appeared to be linked to p75 binding for mutants isolated in DE Rd1, we introduced p75 as a further conformational screening criterion for DE Rd2 in parallel to the use of TrkB alone during the sorting process (Fig. 2A; see Materials and Methods for details). Enriched DE Rd2 pools exhibited additional increases in TrkB binding and full-length expression along with a notable increase in p75 binding. On a clonal mutant BDNF basis, TrkB binding and full-length expression increased together such that the specific activity toward TrkB was not further increased over that for DE Rd1 mutants (Table 2; Fig. 2B). However, regardless of whether p75 was included as a screening criterion in DE Rd2 (e.g., "P" mutants [p75] or "K" mutants [TrkB]), specific activity toward p75 was found to increase an average of 4.1-fold over that for the DE Rd1 clone T5. Sequence analysis revealed that the BDNF mutants selected in DE Rd2 were primarily a result of shuffled combinations of the mutations from DE Rd1 (Table 1). As mentioned above, screens in both DE Rd1 and DE Rd2 were biased toward improvements in folding fidelity rather than toward improvements in affinity by screening using saturating TrkB and p75 concentrations. For confirmation, apparent TrkB binding affinities for several DE Rd1 and Rd2 BDNF mutants were measured, and as expected, apparent TrkB binding affinities were not improved. Instead,

TABLE 2 Binding and expression of BDNF mutants

Characteristic	Value[a] for:											
	Wild type	DE Rd1				DE Rd2						
		T4	T5	B2	B5	P1	P3	P5	P10	K3	K6	K8
Expression[b]	1.0 ± 0.1	1.4 ± 0.1	1.4 ± 0.1	1.4 ± 0.1	2.4 ± 0.1	5.0 ± 0.7	4.2 ± 0.4	4.1 ± 0.2	5.2 ± 0.4	5.1 ± 0.1	3.1 ± 0.3	3.4 ± 0.1
Specific binding activity for:												
TrkB[c]	1.0 ± 0.1	3.1 ± 0.1	3.9 ± 0.3	2.0 ± 0.3	1.5 ± 0.1	2.7 ± 0.3	2.6 ± 0.3	2.7 ± 0.1	2.4 ± 0.1	3.0 ± 0.1	2.9 ± 0.2	4.0 ± 0.3
p75[d]	None	1.6 ± 0.1	1.0 ± 0.1	None	0.6 ± 0.1	5.0 ± 0.9	3.4 ± 0.3	5.9 ± 0.2	4.7 ± 0.5	2.9 ± 0.1	3.4 ± 0.3	3.4 ± 0.3

[a] Fold change, expressed as means ± standard deviations for triplicate independent transformants. Statistically significant differences were found (P, <0.05) for full-length expression and TrkB binding activity between all mutants and wild-type BDNF. Statistically significant differences were also found (P, <0.05) for p75 binding activity between T5 and all other mutants. Statistical evaluation was performed using an unpaired, two-tailed Student t test.

[b] Full-length expression on the yeast surface as determined by c-*myc* epitope labeling and flow cytometry and normalized to that of wild-type BDNF.

[c] As determined by flow cytometry and normalized to the TrkB binding activity of wild-type BDNF.

[d] As determined by flow cytometry and normalized to the p75 binding activity of mutant T5.

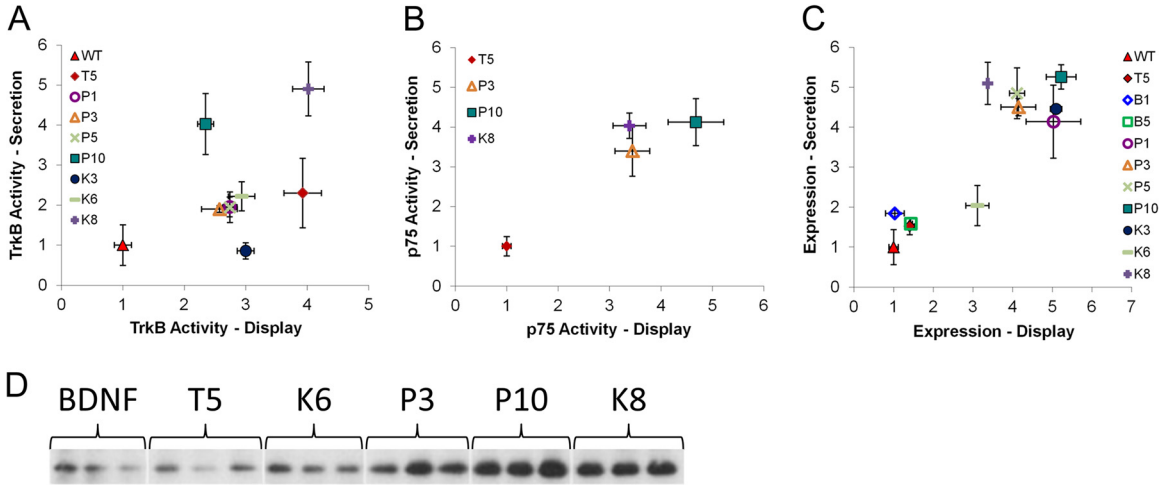

FIG 3 Comparison of the binding and expression properties of displayed and secreted BDNF proteins. (A) Specific binding activity toward the TrkB receptor as measured on the yeast surface by flow cytometry (Display) or for the secreted protein by ELISA (Secretion). TrkB binding activity is expressed per full-length molecule as assessed by the c-*myc* epitope and normalized to wild-type BDNF activity. (B) Specific binding activity toward the p75 receptor, determined as described for the TrkB receptor, and normalized to the activity of the T5 BDNF mutant. (C) Relative expression levels determined by flow cytometry (Display) or Western blotting (Secretion) and normalized to wild-type BDNF expression. In panels A to C, data are expressed as means ± standard deviations for triplicate independent transformants. Statistical evaluation was performed using an unpaired, two-tailed Student *t* test. (D) Sample Western blot data used to generate the relative secretion values reported in panel C.

while the apparent affinities of BDNF mutants remained in the low nanomolar range, they were marginally lower than that of wild-type BDNF (see Fig. S1 in the supplemental material). In summary, each BDNF clone isolated after DE Rd2 demonstrated improved specific activity for both natural receptors, TrkB and p75, likely as a result of improved folding and processing in yeast.

Effects of mutations on the binding activity and expression of surface-displayed and secreted BDNF. To further explore the individual mutants and the effects of certain mutations on expression and specific activity, we compared BDNF mutants as surface-displayed and secreted proteins. Mutagenesis in DE Rd1 served to improve the folding fidelity of BDNF displayed on the yeast surface, as evidenced by improved specific activity toward TrkB and p75, combined with small improvements in the display of the full-length protein (Table 2). By use of receptor-binding ELISAs, secreted DE Rd1 mutant T5 exhibited improved TrkB binding activity over that of wild-type BDNF, and unlike wild-type BDNF, secreted T5 exhibited p75 binding activity, as was observed on the yeast surface (Table 2; Fig. 3A and B). The secreted and surface-displayed protein expression levels correlated quite well for the individual BDNF mutants studied, with 5-fold improvements in the secretion yield for many Rd2 mutants (Fig. 3C and D). However, the specific TrkB binding activity of most Rd2 mutants was not further increased over Rd1 levels either on the surface or for the soluble protein, suggesting that these mutants could be generally classified as "expression" mutants (e.g., Rd2 mutants K6, P5, and P3 [Fig. 3A]). However, when Glu40Asp was present in addition to the "expression" mutations, the specific TrkB binding activity of secreted BDNF protein was improved substantially (Fig. 3A, compare P10 to P5 and K8 to K6 and T5) (P, <0.05). In addition, improved specific p75 binding activity on the yeast surface correlated well with improved binding activity of the secreted protein for those mutants tested (Fig. 3B). Taken together, P10 and K8 had the best combination of expression and binding properties as secreted proteins.

An interesting set of mutations involved cysteine residues that reside proximally to the native cysteines forming the intramolecular cysteine knot disulfide bond architecture (Fig. 4B). The predominant cysteine mutation in DE Rd2 was the Ser11Cys mutation, which is 2 amino acids removed from the native Cys13 residue. The other DE Rd2 cysteine mutation, found only in the K8 mutant, was Gly67Cys, which is directly adjacent to the native Cys68 residue. Cysteines 13 and 68 participate in two different disulfide bonds within the cysteine knot structure (Fig. 4B). To determine the extent of involvement of the cysteine modifications in the improvements observed in BDNF expression and binding activity on the cell surface, we created several additional BDNF mutant constructs with alterations at positions 11, 13, 67, and 68 and analyzed them using yeast surface display (Fig. 5). Beginning with mutant P3, which had the fewest mutations in DE Rd2, the Cys11 mutation was reverted to the wild-type Ser residue (P3 Cys11Ser), and while the specific binding activity toward TrkB was not affected (P, >0.05), the expression level and specific binding activity toward p75 were substantially decreased (P, <0.05). When the Cys67 mutation found in the K8 mutant was added to replace Cys11 in the P3 mutant (P3 Gly67Cys Cys11Ser), the protein expression level and p75 binding activity remained lower than those of the parent, P3 (P, <0.05). There was a small increase in specific binding activity toward TrkB, similar to the increase observed by comparing K8 with the rest of the DE Rd2 mutants, including P3 (Fig. 3A) (P, <0.05). Since Gly67Cys could not complement the effects of Cys11Ser reversion, the Ser11Cys and Gly67Cys mutations appeared to play different roles, at least in the P3 background. Thus, to check for possible synergy of the two Cys mutations, the Gly67Cys mutation was added to the P3 mutant (P3 Gly67Cys), but specific binding activities toward both TrkB and p75 were reduced (P, <0.05). Moreover, knocking out the natural cysteine in either P3 (Cys13Ala) or K8 (Cys68Ala) had substantial detrimental effects on the binding activities for both receptors (P, <0.05), suggesting that neither of the cysteine mu-

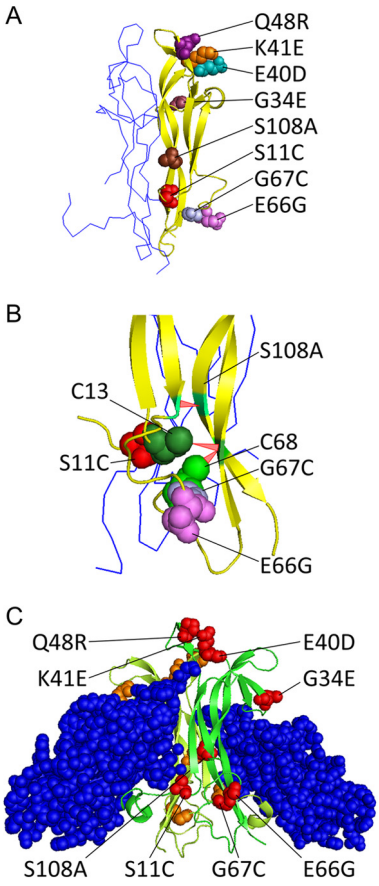

FIG 4 Structural locations of identified mutations. (A) BDNF (yellow) and neurotrophin 4 (blue) heterodimer structure (PDB code 1HCF [42]). Residues subject to mutation in P10 and K8 are highlighted. (B) Enlarged view of cysteine knot protein core highlighting the native Cys13 and Cys68 residues as well as the Ser11Cys and Gly67Cys mutations, along with the three intramolecular disulfide bonds (red lines). (C) Structure of the neurotrophin 4 homodimer (dark and light green) binding to the TrkB receptor (blue) (PDB code 1B8M [10]). The homologous NT4 residues corresponding to the P10 and K8 mutations are highlighted (red and orange).

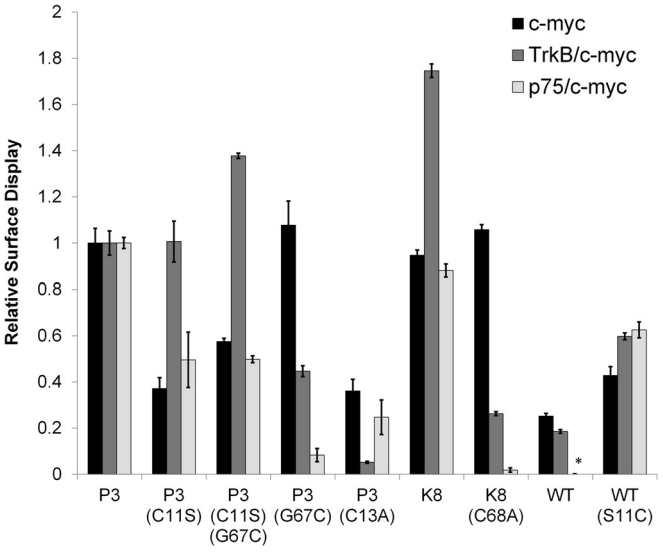

FIG 5 Evaluation of cysteine mutations by site-directed mutagenesis and yeast surface display. Cysteine mutations and reversions were incorporated into the P3, K8, and wild-type BDNF (WT) constructs. Specific binding activities toward p75 and TrkB, along with full-length expression levels (c-*myc*), were measured by flow cytometry. Data are means ± standard deviations for triplicate independent transformants. Statistical evaluation was performed using an unpaired, two-tailed Student *t* test. *, labeling not detected for this construct.

tations was simply replacing the natural cysteine in the disulfide-bonding network. Finally, when the predominant DE Rd2 Ser11Cys mutation was added as the sole mutation to wild-type BDNF, surface expression, along with both TrkB and p75 specific binding activities, was increased over that of wild-type BDNF (P, <0.05), though not to the levels observed for P3. These data indicated that while Ser11Cys is important, other, additional mutations are required for proper BDNF folding and processing to the yeast surface. In addition to the cysteine modifications, the Gly34Glu and Ser108Ala mutations were found in the majority of mutant BDNF constructs isolated, often in coordination with Ser11Cys. Mutant P3 combines these three alterations, and its expression, TrkB binding, and P75 binding properties were all improved, indicating that these constitute a "minimal mutant" that has reasonable expression and binding function both on the surface and as a soluble protein (Table 2 and Fig. 3).

Biologically active BDNF exists as a homodimer held together by hydrophobic interactions, and the TrkB and p75 receptors engage both monomers in a homodimeric pair (10, 37, 38). Thus, we next assessed the preservation of the dimerization interface among the most favorable mutants, K8 and P10, on the yeast surface. First, BDNF dimerization was demonstrated by coexpressing a secreted BDNF construct with a traceable epitope (His_6) simultaneously with the Aga2p-fused surface-tethered construct bearing the c-*myc* epitope tag (Fig. 1Aii). Thus, association between a tethered BDNF monomer and a secreted BDNF monomer could be detected simply by measuring the amount of the His_6 epitope (secreted BDNF) captured on the yeast surface, along with the maintenance of TrkB binding activity. In this way, it was demonstrated that the K8 and P10 mutants associate via putative dimerization, since the secreted forms could be specifically captured on the yeast surface by tethered K8 or P10 (Fig. 6). In contrast, K8 showed no capture of an irrelevant single-chain antibody (4-4-20), nor did display of a highly expressed c-*myc* epitope lead to any K8 capture, indicating that the capture is specific to the pairing of BDNF monomers (Fig. 6). Furthermore, tethered K8 could capture secreted P10 and bind TrkB, indicating that dimerization interactions occur between two distinct mutants and suggesting conservation of the dimerization interface (Fig. 6).

Fidelity and biological activity of secreted BDNF mutants. To further confirm that the BDNF mutants maintained their homodimeric structures, we next purified K8 via the six-histidine tag (purified yield, ~1 mg/liter) and investigated molecular isoforms using size exclusion chromatography (SEC) combined with chemical cross-linking. SEC eluate fractions were subjected to glutaraldehyde cross-linking to investigate monomer, dimer, or higher-order multimer formation. As Fig. 7 indicates, the majority of the secreted K8 protein is in the form of BDNF homodimers, as confirmed by chemical cross-linking prior to Western blot analysis (~70%; 21 to 24 min). A small amount of K8 BDNF is secreted in the form of high-molecular-weight aggregates at early elution times (~15%; 17 to 19 min), and very little is secreted in the form

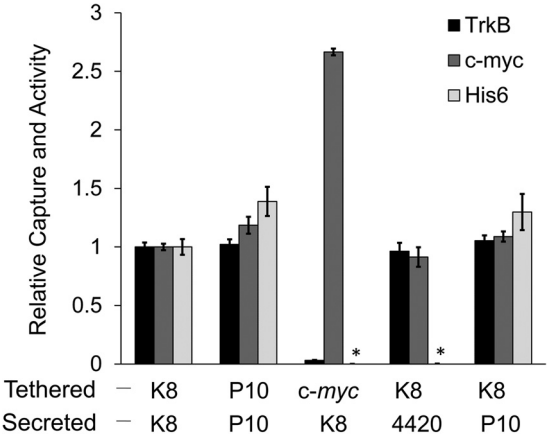

FIG 6 Surface capture of secreted BDNF mutants. Surface display and secretion constructs were coexpressed as indicated in Fig. 1Aii prior to evaluation of TrkB binding and of c-*myc* (tethered display) and His_6 (secreted and captured display) epitope tags by flow cytometry. All labeling is normalized to that for the K8 mutant. The tethered c-*myc* sample is an Aga2p fusion with the c-*myc* epitope (i.e., Fig. 1Aii without the BDNF insertion). The secretion sample (4-4-20) represents an anti-fluorescein single-chain antibody. *, His_6 labeling not detected for these constructs. Data are means ± standard deviations for triplicate independent transformants.

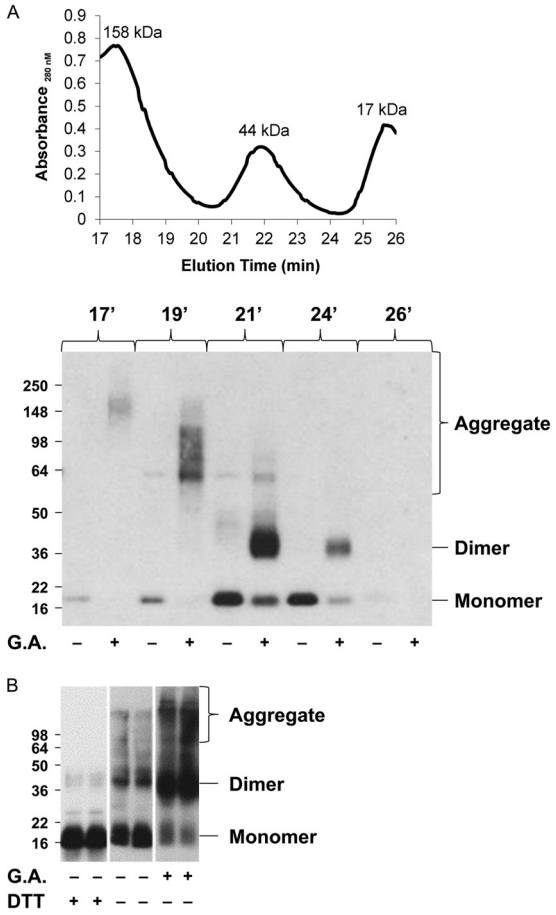

FIG 7 Size exclusion chromatography analysis of the secreted and purified K8 BDNF mutant. (A) (Top) Elution chromatogram of molecular size standards. (Bottom) Western blot of K8 sample eluates aligned by elution time with the molecular size standards. Samples were run under reducing conditions with (+) or without (−) glutaraldehyde (G.A.) cross-linking. (B) Western blot of secreted and purified K8 under both reducing and nonreducing SDS-PAGE conditions (with and without DTT) and with and without cross-linking (with and without G.A.). A slightly overexposed blot is presented to allow viewing of all BDNF species.

of monomers (~2%; 26 min). Finally, examination of the secretion product by Western blotting in the presence or absence of a reducing agent (DTT) and cross-linking indicates the presence of homodimers (Fig. 7B, +G.A. −DTT) that can be disrupted by SDS treatment (Fig. 7B, −G.A. −DTT), indicating hydrophobic homodimerization as opposed to any newly introduced disulfide-based dimerization via the Gly67Cys mutation. Taken together, these experiments indicate that the secreted mutant BDNF exists largely as noncovalent homodimers, contrasting significantly with the large disulfide-bonded aggregates observed for secreted wild-type BDNF (Fig. 1C).

Finally, in addition to the ELISA-based binding activity demonstrated for secreted BDNF mutants, the K8 and P10 BDNF mutants were tested for their abilities to elicit biological activity in the form of intracellular phosphorylation of TrkB receptors. The K8 and P10 proteins were purified and were added to prestarved TrkB-transfected rat adrenal pheochromocytoma cells (PC12 cells) (35). Following immunoprecipitation of TrkB receptors, receptor phosphorylation was evaluated by Western blotting. Both K8 and P10 promoted specific phosphorylation of the full-length TrkB receptor (Fig. 8).

DISCUSSION

In this report, the yeast display and secretion properties of BDNF were improved substantially through directed evolution. Wild-type BDNF was secreted in small quantities as a misfolded aggregate capable in some way of evading the normally stringent yeast quality control mechanisms (39). Similarly, wild-type BDNF was expressed at relatively low levels on the yeast cell surface, and while it was capable of binding TrkB, binding to p75 was not detected. The ability of misfolded heterologous proteins to overcome yeast quality control is not unique to BDNF and has been observed for the display of the epidermal growth factor receptor extracellular domain and binding loop-inserted green fluorescent proteins, which were expressed on the yeast cell surface in a partially misfolded state (21, 23). During DE Rd1, it was discovered that the BDNF mutants were better displayed on the yeast surface, possessed better specific binding activity toward TrkB, and, unlike wild-type BDNF, could bind the p75 receptor. During DE Rd2, several mutants whose increased specific binding activities to

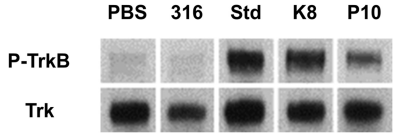

FIG 8 TrkB phosphorylation by the K8 and P10 BDNF mutants. TrkB-transfected PC12 cells were exposed to commercial wild-type BDNF (Std), the BDNF mutant K8, the BDNF mutant P10, and two negative controls: a yeast supernatant from cells containing an empty secretion vector (designated 316) and a saline-treated sample (PBS). Western blotting of the pan-Trk-immunoprecipitated product with detection of either the phosphorylated TrkB receptor (P-TrkB) or the total Trk receptor (Trk) was performed. Bands corresponding to the full-length TrkB receptor at ~145 kDa are shown.

TrkB and p75 translated well from the yeast surface to the secreted protein were identified. In particular, the improved properties of mutants K8 and P10 as secreted proteins appeared to be driven at least in part by the Glu40Asp mutation (Fig. 4A). This fairly conservative mutation is localized to the solvent-exposed BDNF surface outside the putative TrkB and p75 binding sites (10, 37), suggesting that the improvements in specific TrkB and p75 binding activities may result from an important role of the Glu40Asp mutation in locking in the folded conformation of the secreted BDNF. Mutant K8 was secreted at 1 mg/liter, and the formation of high-molecular-weight aggregates in the secreted product was substantially decreased from that for wild-type BDNF (compare Fig. 7B, −DTT lanes, with Fig. 1C); the majority of the material was produced in dimeric form, as evidenced by chemical cross-linking experiments. Additionally, the secreted K8 and P10 mutants were both capable of triggering receptor phosphorylation in a cellular context. Taken together, these evolved BDNF mutants are capable of overcoming deficits in yeast secretory processing to exhibit much better expression, folding fidelity, and activity than wild-type BDNF.

In addition to the key Glu40Asp mutant, all DE Rd2 mutants possessed a cysteine mutation at amino acid position 11 (Ser11Cys) or 67 (Gly67Cys), positions that are proximal to the native cysteine residues at positions 13 and 68, respectively (Fig. 4B). The native Cys13 and Cys68 residues are involved in two of the three intramolecular disulfide bonds that constitute the cysteine knot configuration of each BDNF monomer (40). Analysis of the receptor-binding properties of P3 in which the native Cys13 is changed to alanine or K8 in which the native Cys68 is changed to alanine showed substantial deficits in folding and expression, indicating that these native cysteine residues remain crucial for mutant BDNF processing. Moreover, reversion of the Ser11Cys mutation was detrimental to expression and overall folding for P3 BDNF, indicating the specific impact of this mutation. The Ser11Cys mutation is a conservative change in terms of physiochemical properties, aside from the ability to participate in disulfide bonds. Moreover, the aforementioned processing deficits upon mutation of the native cysteines also suggested that the native cysteines are not likely replaced in the disulfide bond network by the proximal Ser11Cys or Gly67Cys mutation in P3 or K8, respectively. An additional possibility is for the new proximal cysteine residues to drive homodimer assembly by intermolecular disulfide bonding. However, nonreducing Western blotting indicated that the homodimeric interactions of the BDNF mutants were hydrophobic in nature, and the mutations instead substantially reduced the aberrant disulfide-bonded aggregates observed for wild-type BDNF. Thus, it may be plausible that the new proximal cysteine residues provided by Ser11Cys or Gly67Cys enable transient nonnative disulfide formation in productive folding intermediates that yield more-efficient native disulfide pairing, although further detailed study would be required to test this hypothesis. In addition, the Glu66Gly mutation just 2 residues removed from the native Cys68 was present in many DE Rd2 mutants, such as P10. However, the Glu66Gly mutation did not appear in concert with the Gly67Cys mutation, perhaps indicating that this region of the protein offered structural challenges to folding that could be addressed by either mutation. As a comparative example, yeast display and directed evolution of the tumor necrosis factor receptor identified expression-enhancing proline mutations that helped lock adjacent cysteine residues into correct orientations for disulfide bonding (41). Finally, when Ser11Cys was introduced as the only mutation into wild-type BDNF, the protein was better expressed and could bind both TrkB and p75, but not to the level of P3, indicating that other mutations arising from the DE process are playing important roles.

Examination of the mutations in K8 and P10 indicates that they are all located in BDNF regions that are not predicted to make contact with TrkB, based on BDNF and neurotrophin 4 (NT4) structural homology in combination with the solved NT4–TrkB structure (Fig. 4C) (10, 42). The identification of mutations that all lie outside of the putative BDNF-TrkB interface (10) suggested that screening at saturating receptor concentrations was effective in identifying better-folded mutants while avoiding the selection of mutants with improved receptor-binding affinity. Indeed, while BDNF mutation improved the specific activity toward TrkB (binding per molecule), affinity measurements indicated some decrease in the apparent TrkB binding affinities (K_D) for the mutant BDNF constructs, although they still remained in the low nanomolar range, as previously reported (43, 44). If critical, the BDNF binding affinity to its receptors could always be improved as desired in further protein engineering efforts (30, 45).

Residues Glu40, Lys41, and Gln48 were previously shown to be part of a BDNF loop region that, when swapped into a BDNF-NGF chimera, could help improve the TrkB binding and activity of the chimeric molecule, indicating an ability to affect the folded conformation (46, 47). Moreover, during loop-swapping experiments, expression levels were also diminished, suggesting that this loop region can affect expression as well (46). Comparing our findings with these observations, we found that mutations in the same loop region were capable of improving the protein expression and specific activity of BDNF toward the TrkB receptor, likely through improved folding fidelity. Each of the Glu40Asp, Lys41Glu, and Gln48Arg mutations incorporates an amino acid with side-chain properties that lead to an addition or change of charge in these solvent-exposed residues. Mutational change to charged residues at solvent-exposed protein interfaces has been shown previously to elicit improvements in the expression, stability, activity, and solubility of engineered proteins (19, 48).

Finally, Ser108 is located within the highly conserved hydrophobic interface that leads to neurotrophin homodimer formation (49), and most of the DE Rd2 mutants, including K8 and P10, contain the Ser108Ala mutation (Fig. 4A). The addition of another nonpolar hydrophobic residue could possibly help promote proper neurotrophin assembly by influencing the hydrophobic dimerization interface. Interestingly, while BDNF and NT3 have a serine at position 108, NGF and NT4 possess an alanine at this position, and it is known that BDNF can heterodimerize with both NT3 and NT4 (42, 49), indicating that the Ser108Ala change is tolerated at the interface. Indeed, the homodimeric (K8–K8 and P10–P10) and heterodimeric (K8–P10) pairing of the BDNF mutants by surface capture indicated maintenance of the hydrophobic dimerization interface in the presence of the Ser108Ala mutation, as well as the other mutations present in the K8 and P10 versions of BDNF. In conclusion, this work demonstrates that yeast surface display combined with directed evolution can be used to improve the expression and folding properties of BDNF. Moreover, the successful surface display of well-folded BDNF will enable the use of the yeast display protein engineering toolkit for applications such as neurotrophin affinity maturation, stability engineering, and epitope mapping.

ACKNOWLEDGMENTS

We thank Eric Shooter for the generous donation of the TrkB-transfected PC12 cell line.

This work was supported by National Science Foundation grants BES-0238864 and CBET-0853801. M.L.B. was supported by a National Institutes of Health Clinical Neuroengineering Training Program grant (T90 DK07007), and T.M.M. was supported by a National Science Foundation graduate fellowship.

REFERENCES

1. **Pezet S, Malcangio M.** 2004. Brain-derived neurotrophic factor as a drug target for CNS disorders. Expert Opin. Ther. Targets **8:**391–399. http://dx.doi.org/10.1517/14728222.8.5.391.
2. **Tapia-Arancibia L, Rage F, Givalois L, Arancibia S.** 2004. Physiology of BDNF: focus on hypothalamic function. Front. Neuroendocrinol. **25:**77–107. http://dx.doi.org/10.1016/j.yfrne.2004.04.001.
3. **Zhang Y, Pardridge WM.** 2006. Blood–brain barrier targeting of BDNF improves motor function in rats with middle cerebral artery occlusion. Brain Res. **1111:**227–229. http://dx.doi.org/10.1016/j.brainres.2006.07.005.
4. **Nagahara AH, Merrill DA, Coppola G, Tsukada S, Schroeder BE, Shaked GM, Wang L, Blesch A, Kim A, Conner JM, Rockenstein E, Chao MV, Koo EH, Geschwind D, Masliah E, Chiba AA, Tuszynski MH.** 2009. Neuroprotective effects of brain-derived neurotrophic factor in rodent and primate models of Alzheimer's disease. Nat. Med. **15:**331–337. http://dx.doi.org/10.1038/nm.1912.
5. **Tsukahara T, Takeda M, Shimohama S, Ohara O, Hashimoto N.** 1995. Effects of brain-derived neurotrophic factor on 1-methyl-4-phenyl-1,2,3,6-tetrahydropyridine-induced Parkinsonism in monkeys. Neurosurgery **37:**733–741. http://dx.doi.org/10.1227/00006123-199510000-00018.
6. **Canals JM, Pineda JR, Torres-Peraza JF, Bosch M, Martín-Ibañez R, Muñoz MT, Mengod G, Ernfors P, Alberch J.** 2004. Brain-derived neurotrophic factor regulates the onset and severity of motor dysfunction associated with enkephalinergic neuronal degeneration in Huntington's disease. J. Neurosci. **24:**7727–7739. http://dx.doi.org/10.1523/JNEUROSCI.1197-04.2004.
7. **Jeong HH, Piao S, Ha JN, Kim IG, Oh SH, Lee JH, Cho HJ, Hong SH, Kim SW, Lee JY.** 2013. Combined therapeutic effect of udenafil and adipose-derived stem cell (ADSC)/brain-derived neurotrophic factor (BDNF)–membrane system in a rat model of cavernous nerve injury. Urology **81:**1108.e7–1108.e14. http://dx.doi.org/10.1016/j.urology.2013.01.022.
8. **Barbacid M.** 1994. The Trk family of neurotrophin receptors. J. Neurobiol. **25:**1386–1403. http://dx.doi.org/10.1002/neu.480251107.
9. **Heumann R.** 1994. Neurotrophin signalling. Curr. Opin. Neurobiol. **4:**668–679. http://dx.doi.org/10.1016/0959-4388(94)90008-6.
10. **Banfield MJ, Naylor RL, Robertson AG, Allen SJ, Dawbarn D, Brady RL.** 2001. Specificity in Trk receptor:neurotrophin interactions: the crystal structure of TrkB-d5 in complex with neurotrophin-4/5. Structure **9:**1191–1199. http://dx.doi.org/10.1016/S0969-2126(01)00681-5.
11. **Butte MJ, Hwang PK, Mobley WC, Fletterick RJ.** 1998. Crystal structure of neurotrophin-3 homodimer shows distinct regions are used to bind its receptors. Biochemistry **37:**16846–16852. http://dx.doi.org/10.1021/bi981254o.
12. **Wiesmann C, Ultsch MH, Bass SH, de Vos AM.** 1999. Crystal structure of nerve growth factor in complex with the ligand-binding domain of the TrkA receptor. Nature **401:**184–188. http://dx.doi.org/10.1038/43705.
13. **Colangelo AM, Finotti N, Ceriani M, Alberghina L, Martegani E, Aloe L, Lenzi L, Levi-Montalcini R.** 2005. Recombinant human nerve growth factor with a marked activity in vitro and in vivo. Proc. Natl. Acad. Sci. U. S. A. **102:**18658–18663. http://dx.doi.org/10.1073/pnas.0508734102.
14. **Philo JS, Rosenfeld R, Arakawa T, Wen J, Narhi LO.** 1993. Refolding of brain-derived neurotrophic factor from guanidine hydrochloride: kinetic trapping in a collapsed form which is incompetent for dimerization. Biochemistry **32:**10812–10818. http://dx.doi.org/10.1021/bi00091a036.
15. **Hoshino K, Eda A, Kurokawa Y, Shimizu N.** 2002. Production of brain-derived neurotrophic factor in *Escherichia coli* by coexpression of Dsb proteins. Biosci. Biotechnol. Biochem. **66:**344–350. http://dx.doi.org/10.1271/bbb.66.344.
16. **Fandl JP, Tobkes NJ, McDonald NQ, Hendrickson WA, Ryan TE, Nigam S, Acheson A, Cudny H, Panayotatos N.** 1994. Characterization and crystallization of recombinant human neurotrophin-4. J. Biol. Chem. **269:**755–759.
17. **Nishizawa M, Ozawa F, Higashizaki T, Hirai K, Hishinuma F.** 1993. Biologically active human and mouse nerve growth factors secreted by the yeast *Saccharomyces cerevisiae*. Appl. Microbiol. Biotechnol. **38:**624–630.
18. **Fukuzono S, Fujimori K, Shimizu N.** 1995. Production of biologically active mature brain-derived neurotrophic factor in *Escherichia coli*. Biosci. Biotechnol. Biochem. **59:**1727–1731. http://dx.doi.org/10.1271/bbb.59.1727.
19. **Shusta EV, Holler PD, Kieke MC, Kranz DM, Wittrup KD.** 2000. Directed evolution of a stable scaffold for T-cell receptor engineering. Nat. Biotechnol. **18:**754–759. http://dx.doi.org/10.1038/77325.
20. **Traxlmayr MW, Faissner M, Stadlmayr G, Hasenhindl C, Antes B, Rüker F, Obinger C.** 2012. Directed evolution of stabilized IgG1-Fc scaffolds by application of strong heat shock to libraries displayed on yeast. Biochim. Biophys. Acta **1824:**542–549. http://dx.doi.org/10.1016/j.bbapap.2012.01.006.
21. **Kim YS, Bhandari R, Cochran JR, Kuriyan J, Wittrup KD.** 2006. Directed evolution of the epidermal growth factor receptor extracellular domain for expression in yeast. Proteins **62:**1026–1035. http://dx.doi.org/10.1002/prot.20618.
22. **Pepper LR, Cho YK, Boder ET, Shusta EV.** 2008. A decade of yeast surface display technology: where are we now? Comb. Chem. High Throughput Screen. **11:**127–134. http://dx.doi.org/10.2174/138620708783744516.
23. **Pavoor TV, Cho YK, Shusta EV.** 2009. Development of GFP-based biosensors possessing the binding properties of antibodies. Proc. Natl. Acad. Sci. U. S. A. **106:**11895–11900. http://dx.doi.org/10.1073/pnas.0902828106.
24. **Huang D, Shusta EV.** 2005. Secretion and surface display of green fluorescent protein using the yeast *Saccharomyces cerevisiae*. Biotechnol. Prog. **21:**349–357. http://dx.doi.org/10.1021/bp0497482.
25. **Wentz AE, Shusta EV.** 2007. A novel high-throughput screen reveals yeast genes that increase secretion of heterologous proteins. Appl. Environ. Microbiol. **73:**1189–1198. http://dx.doi.org/10.1128/AEM.02427-06.
26. **Boder ET, Wittrup KD.** 1997. Yeast surface display for screening combinatorial polypeptide libraries. Nat. Biotechnol. **15:**553–557. http://dx.doi.org/10.1038/nbt0697-553.
27. **Gietz RD, Woods RA.** 2002. Transformation of yeast by lithium acetate/single-stranded carrier DNA/polyethylene glycol method. Methods Enzymol. **350:**87–96. http://dx.doi.org/10.1016/S0076-6879(02)50957-5.
28. **Watson JV.** 1992. Flow cytometry data analysis: basic concepts and statistics. Cambridge University Press, Cambridge, United Kingdom.
29. **Tillotson BJ, Cho YK, Shusta EV.** 2013. Cells and cell lysates: a direct approach for engineering antibodies against membrane proteins using yeast surface display. Methods **60:**27–37. http://dx.doi.org/10.1016/j.ymeth.2012.03.010.
30. **Colby DW, Kellogg BA, Graff CP, Yeung YA, Swers JS, Wittrup KD.** 2004. Engineering antibody affinity by yeast surface display. Methods Enzymol. **388:**348–358. http://dx.doi.org/10.1016/S0076-6879(04)88027-3.
31. **Swers JS, Kellogg BA, Wittrup KD.** 2004. Shuffled antibody libraries created by in vivo homologous recombination and yeast surface display. Nucleic Acids Res. **32:**e36. http://dx.doi.org/10.1093/nar/gnh030.
32. **Zaccolo M, Williams DM, Brown DM, Gherardi E.** 1996. An approach to random mutagenesis of DNA using mixtures of triphosphate derivatives of nucleoside analogues. J. Mol. Biol. **255:**589–603. http://dx.doi.org/10.1006/jmbi.1996.0049.
33. **Stemmer WP.** 1994. DNA shuffling by random fragmentation and reassembly: in vitro recombination for molecular evolution. Proc. Natl. Acad. Sci. U. S. A. **91:**10747–10751. http://dx.doi.org/10.1073/pnas.91.22.10747.
34. **Jaboin J, Kim CJ, Kaplan DR, Thiele CJ.** 2002. Brain-derived neurotrophic factor activation of TrkB protects neuroblastoma cells from chemotherapy-induced apoptosis via phosphatidylinositol 3′-kinase pathway. Cancer Res. **62:**6756–6763.
35. **Kaplan DR, Hempstead BL, Martin-Zanca D, Chao MV, Parada LF.** 1991. The *trk* proto-oncogene product: a signal transducing receptor for nerve growth factor. Science **252:**554–558. http://dx.doi.org/10.1126/science.1850549.
36. **Vesa J, Kruttgen A, Shooter EM.** 2000. p75 reduces TrkB tyrosine autophosphorylation in response to brain-derived neurotrophic factor and neurotrophin 4/5. J. Biol. Chem. **275:**24414–24420. http://dx.doi.org/10.1074/jbc.M001641200.
37. **He XL, Garcia KC.** 2004. Structure of nerve growth factor complexed with the shared neurotrophin receptor p75. Science **304:**870–875. http://dx.doi.org/10.1126/science.1095190.

38. **Pattarawarapan M, Burgess K.** 2003. Molecular basis of neurotrophin-receptor interactions. J. Med. Chem. **46:**5277–5291. http://dx.doi.org/10.1021/jm030221q.
39. **Ellgaard L, Helenius A.** 2003. Quality control in the endoplasmic reticulum. Nat. Rev. Mol. Cell Biol. **4:**181–191. http://dx.doi.org/10.1038/nrm1052.
40. **Acklin C, Stoney K, Rosenfeld RA, Miller JA, Rohde MF, Haniu M.** 1993. Recombinant human brain-derived neurotrophic factor (rHuBDNF). Disulfide structure and characterization of BDNF expressed in CHO cells. Int. J. Pept. Protein Res. **41:**548–552.
41. **Schweickhardt RL, Jiang X, Garone LM, Brondyk WH.** 2003. Structure-expression relationship of tumor necrosis factor receptor mutants that increase expression. J. Biol. Chem. **278:**28961–28967. http://dx.doi.org/10.1074/jbc.M212019200.
42. **Robinson RC, Radziejewski C, Spraggon G, Greenwald J, Kostura MR, Burtnick LD, Stuart DI, Choe S, Jones EY.** 1999. The structures of the neurotrophin 4 homodimer and the brain-derived neurotrophic factor/neurotrophin 4 heterodimer reveal a common Trk-binding site. Protein Sci. **8:**2589–2597.
43. **Naylor RL, Robertson AG, Allen SJ, Sessions RB, Clarke AR, Mason GG, Burston JJ, Tyler SJ, Wilcock GK, Dawbarn D.** 2002. A discrete domain of the human TrkB receptor defines the binding sites for BDNF and NT-4. Biochem. Biophys. Res. Commun. **291:**501–507. http://dx.doi.org/10.1006/bbrc.2002.6468.
44. **Dechant G, Biffo S, Okazawa H, Kolbeck R, Pottgiesser J, Barde YA.** 1993. Expression and binding characteristics of the BDNF receptor chick *trkB*. Development **119:**545–558.
45. **Boder ET, Midelfort KS, Wittrup KD.** 2000. Directed evolution of antibody fragments with monovalent femtomolar antigen-binding affinity. Proc. Natl. Acad. Sci. U. S. A. **97:**10701–10705. http://dx.doi.org/10.1073/pnas.170297297.
46. **Ibanez CF, Ilag LL, Murray-Rust J, Persson H.** 1993. An extended surface of binding to Trk tyrosine kinase receptors in NGF and BDNF allows the engineering of a multifunctional pan-neurotrophin. EMBO J. **12:**2281–2293.
47. **Ibanez CF, Ebendal T, Persson H.** 1991. Chimeric molecules with multiple neurotrophic activities reveal structural elements determining the specificities of NGF and BDNF. EMBO J. **10:**2105–2110.
48. **Nieba L, Honegger A, Krebber C, Pluckthun A.** 1997. Disrupting the hydrophobic patches at the antibody variable/constant domain interface: improved in vivo folding and physical characterization of an engineered scFv fragment. Protein Eng. **10:**435–444. http://dx.doi.org/10.1093/protein/10.4.435.
49. **Robinson RC, Radziejewski C, Stuart DI, Jones EY.** 1995. Structure of the brain-derived neurotrophic factor/neurotrophin 3 heterodimer. Biochemistry **34:**4139–4146. http://dx.doi.org/10.1021/bi00013a001.